

# A SiPM-based ZnS:<sup>6</sup>LiF scintillation neutron detector

A. Stoykov, J.-B. Mosset, U. Greuter, M. Hildebrandt, N. Schlumpf

Paul Scherrer Institut, CH-5232 Villigen PSI, Switzerland

In the work presented here we built and evaluated a single-channel neutron detection unit consisting of a ZnS:<sup>6</sup>LiF scintillator with embedded WLS fibers readout by a SiPM. The unit has a sensitive volume of  $2.4 \times 2.8 \times 50 \text{ mm}^3$ ; 12 WLS fibers of diameter 0.25 mm are uniformly distributed over this volume and are coupled to a  $1 \times 1 \text{ mm}^2$  active area SiPM. We report the following performance parameters: neutron detection efficiency  $\sim 65 \%$  at  $1.2 \text{ \AA}$ , background count rate  $< 10^{-3} \text{ Hz}$ , gamma-sensitivity with <sup>60</sup>Co source  $< 10^{-6}$ , dead time  $\sim 20 \mu\text{s}$ , multi-count ratio  $< 1 \%$ . All these parameters were achieved up to the SiPM dark count rate of  $\sim 2 \text{ MHz}$ .

We consider such detection unit as an elementary building block for realization of one-dimensional multichannel detectors for applications in the neutron scattering experimental technique. The dimensions of the unit and the number of embedded fibers can be varied to meet the specific application requirements. The upper limit of  $\sim 2 \text{ MHz}$  on the SiPM dark count rate allows to use SiPMs with larger active areas if required.

*Keywords:* SiPM, MPPC, neutron detector, ZnS:<sup>6</sup>LiF scintillator, WLS fiber

## 1 Introduction

Helium-3 has been for several decades the most widely used converting material in detectors for neutron scattering experiments. The world-wide shortage of its supply starting in 2009 increased significance and stimulated further development of alternative detector technologies [1]. One of these alternatives is the scintillation technology based on ZnS:<sup>6</sup>LiF or ZnS:<sup>10</sup>B<sub>2</sub>O<sub>3</sub> scintillators read out by wavelength-shifting (WLS) fibers [1, 2]. Currently all detectors of this kind utilize photomultiplier tubes (PMTs) or multi-anode photomultiplier tubes (MaPMTs) as photosensors.

The application of silicon photomultipliers (SiPMs) in such detectors has been hindered by their orders of magnitude higher dark count rate at room temperature: the long emission time of the neutron scintillator and the deficient light collection due to its poor transparency made it difficult to combine a high trigger efficiency for the neutron signals with a reasonable suppression of the SiPM dark counts. As mentioned in [2], the solution of this problem requires an improvement of the light collection from the scintillator. In [3, 4, 5] we presented a practical way how to combine this requirement with a small active area of a SiPM. Also we developed an approach to the signal processing based on “digitization” of the SiPM one-electron signals (one primary electron = one standard pulse) followed by a pulse-train analysis to identify the neutron related pulse sequences against the background of the SiPM dark counts.

In this work we built a single-channel detection unit with SiPM readout (prototype units of 1/4 height were used in [3, 4, 5]) and characterized its performance by determining such parameters as trigger efficiency, background count rate, gamma-sensitivity, dead time, and multi-count ratio.

## 2 Detection unit

Figure 1 shows a cross-section of the sensitive volume of the detection unit. The unit consists of four times two layers (thickness 0.25 mm and 0.45 mm) of ZnS:<sup>6</sup>LiF scintillation material (ND2:1 neutron detection screens from Applied Scintillation Technologies [6]) glued together using EJ-500 optical epoxy from Eljen [7]. Twelve WLS fibers Y11(400)M from Kuraray [8] are glued with the same epoxy into the grooves machined in the thicker layers. Compared to [3, 4, 5] we use here WLS fibers with twice higher dye concentration (400 ppm instead of 200 ppm). This increases the light yield by about 20 %. At one side of the unit the fibers are cut along its edge and polished. An aluminized Mylar foil serving as specular reflector is glued on these polished fiber ends to increase the light yield at the other fiber ends which are connected to a SiPM. The total volume of the unit is  $2.4 \times 2.8 \times 50 \text{ mm}^3$  (width x height x length). The net absorption volume excluding grooves with the fibers (effective volume) amounts to 0.83 of this value.

The free ends of the WLS fibers are bundled and glued together into  $\varnothing 1.1 \text{ mm}$  hole in a Plexiglas holder and polished afterwards. The coupling to a  $1 \times 1 \text{ mm}^2$  active area SiPM is done via a so-called optical expander (short  $\varnothing 1.2 \text{ mm}$  clear multicladd fiber) to ensure a uniform illumination of the SiPM sensitive area. Note that the scintillation light from a neutron absorption event is not distributed uniformly over the 12 WLS fibers but is rather concentrated in one or few of them.

The width and the height of this detection unit satisfy the requirements of the POLDI time-of-flight diffractometer concerning the channel pitch (2.5 mm) and the neutron absorption probability ( $\sim 80 \%$  at  $1.2 \text{ \AA}$ ) [5]. A one-dimensional array of 400 such units of 200 mm length arranged along a circle of 2 m radius will constitute one detector module of the POLDI instrument (in total the instrument will be equipped with four such modules). The 50 mm length of the unit in the present work is chosen arbitrarily: we do not expect variations in the performance of the detector and complications in the manufacturing process changing later to the length of 200 mm.

## 3 Signal processing

The used SiPM is a  $1 \times 1 \text{ mm}^2$  active area MPPC S12571-025C from Hamamatsu [9]. It is operated at an overvoltage of 2.5 V at room temperature. The dark count rate is about 100 kHz. Higher dark count rates were induced by illuminating the SiPM with a weak constant light source. The necessity to evaluate the performance of the detector at the dark count rates substantially higher than 100 kHz is motivated by the following considerations. First, even though  $1 \text{ mm}^2$  active area SiPMs with such low dark count rates start to be commonly available, our goal is to develop a detector which will fulfil the performance requirements with different types of SiPMs, e.g. devices with higher intrinsic dark count rates or larger active areas. And second, depending on the radiation environment, the dark count rate of the SiPM might increase with time conditioned by an increase of the concentration of radiation defects in silicon [10]. For example, indicated by long-term measurements in the POLDI experimental area we expect an increase of the SiPM dark count rate of about  $100 \text{ kHz/mm}^2$  per year.

Figure 2 shows the block-diagram of the signal-processing chain including a high bandwidth amplifier, a leading-edge discriminator, an analyzer (designated here as filter), and an event generator unit.

Figure 3 shows an oscilloscope “screen-short” (persistence mode) of the amplified and shaped SiPM signals (SA) and the generated discriminator signals (SD). The discrimination threshold is set low enough so that all SA-signals are accepted. Independent of how many SiPM cells are triggered simultaneously by SiPM cell-to-cell cross-talk per initial single primary charge carrier in one cell (see multiple amplitudes of SA signals), after the discriminator the relation “one primary charge carrier = one standard SD pulse” is always given. This kind of “digitization” suppresses the cross-talk events, which is essential to achieve low background count rate of the detector [5], and allows for further signal processing schemes independent of the used SiPM type.

The SD pulse sequence is processed by the analyzer unit. Approaches for the realization of the analyzer can be chosen differently as described in [3, 4, 5]. In the current case we use a multistage “single-pulse elimination” filter described in [4] to extract the neutron signals from the dark-count background. The tunable parameters of the filter, defining the detection threshold, are the number of filtering stages  $N$  and the width of the internal gate signals for the first and the following filter stages:  $\text{gate}(1)$  and  $\text{gate}(2..N)$ . The dark count rejection is dominated by the gate width of the first filter stage and by the total number of consecutive stages, while for better transmission of the “extended” pulse trains corresponding to neutron scintillation events longer gate values for the following stages are advantageous. In this study, the filter time constants  $\text{gate}(2..N)$  were fixed to 500 ns, while the parameters  $\text{gate}(1)$  and  $N$  were varied.

Figure 4 shows an example of SD pulse sequence and of corresponding SF pulse sequence from the filter as a result of “identification” of one neutron scintillation event. The first pulse of the SF-signal triggers the event generator (a retriggerable mono-flop with adjustable pulse width) which generates an event signal SN. For the duration of the SN signal the system is blocked – no second pulse can be generated. Such blocking is necessary to account for the long afterglow of the scintillator and prevents multiple triggers from the same scintillation event. The actual blocking time is automatically adjusted in accordance with the strength of the signal at the filter output and is equal or longer than its initial set value (b-time). The parameter b-time was varied in the present measurements in the range from  $5 \mu\text{s}$  to  $200 \mu\text{s}$ .

## 4 Measurements

### 4.1 Trigger Efficiency

The measurements were performed with a  $^{241}\text{AmBe}$  neutron source (intensity  $2 \cdot 10^4$  fast neutrons per second) positioned in the center of a  $0.8 \times 0.8 \times 0.8 \text{ m}^3$  moderator block made of polyethylene. The detection unit was placed in a distance of  $\sim 5 \text{ cm}$  from the source in a slot made in the moderator block. To shield the detector from 60 keV gamma photons accompanying the alpha-decay of  $^{241}\text{Am}$ , the source was shielded by placing it inside a cylindrical tube made of lead with 5 mm thick walls.

To estimate the neutron absorption rate in the detection unit a calibration measurement with a low threshold ( $\text{gate}(1) = 80 \text{ ns}$ ,  $N = 4$ ) was performed. Figure 5 shows the distribution of the number of SD-counts in the first  $10 \mu\text{s}$  of the signals. The trigger efficiency of 0.92 is obtained as the ratio of the number of events in this measured histogram to that in the histogram obtained by extrapolating the measured histogram to zero number of SD-counts. Taking into account the measured event rate of 8.3 Hz the neutron absorption

rate in the detection unit is estimated to be 9.0 Hz. In the following measurements the trigger efficiency was determined as the ratio of the measured event rate to this neutron absorption rate.

Figure 6 shows the trigger efficiency as a function of the filter parameters gate(1) and N. By decreasing gate(1) and increasing N we increase the strength of the filter and thus decrease its trigger efficiency. The operation point was chosen at gate(1) = 30 ns and N = 10 which ensures the trigger efficiency at the level of 80 %. Combined with the neutron absorption probability of  $\sim 80\%$  at 1.2 Å (see above) this gives the neutron detection efficiency of  $\sim 65\%$  at this wavelength.

## 4.2 Background Count Rate

Figure 7 shows the background count rate of the detector as a function of the number of filter stages for three different values (100 kHz, 1000 kHz, and 2000 kHz) of SiPM dark count rates. At the chosen operation point, where we reach a trigger efficiency around 80 %, the background count rate below  $10^{-3}$  Hz is achieved for SiPM dark count rates of up to  $\sim 2$  MHz.

## 4.3 Gamma Sensitivity

The gamma-sensitivity was measured with a  $^{60}\text{Co}$  source. The source is point-like and incorporated into a tablet of  $\varnothing = 25$  mm. Its activity is  $\sim 60$  kBq. The rate of  $\sim 1.3$  MeV photons passing through our 2.4 mm wide detection unit was estimated to be  $10^4 \text{ s}^{-1}$ . This calibration was done with a  $2 \times 2 \times 12 \text{ mm}^3$  LYSO crystal mounted onto a photocathode of a PMT: with the low detection threshold the rate of gamma-events was measured to be  $\sim 10^3 \text{ s}^{-1}$  and the interaction probability for 1.3 MeV photons in 2 mm thick LYSO material was taken as 10 % [11].

Figure 8 shows the gamma-sensitivity as a function of the number of filter stages at different SiPM dark count rates. The probability to trigger on gamma-events is enhanced by the presence of dark counts and the gamma-sensitivity increases with increasing the dark count rate. At the chosen operation point the gamma-sensitivity amounts to  $3 \cdot 10^{-8}$ ,  $10^{-7}$ , and  $8 \cdot 10^{-7}$  at the SiPM dark count rates of 140 kHz, 1000 kHz, and 2000 kHz, respectively.

## 4.4 Multi-Count Ratio

Figure 9 shows the multi-count ratio of the detector as a function of the set value of the blocking time (b-time) of the event generator. The multi-count ratio is defined [12] as the ratio between the measured and the true number of neutron events minus 1. For the true number of neutron events we take the value measured with b-time =  $200 \mu\text{s}$ . Down to b-time =  $15 \mu\text{s}$  the multi-count ratio remains zero within the experimental accuracy of  $\sim 0.05\%$ . Below  $15 \mu\text{s}$  the multi-count ratio starts to increase and reaches the level of 1 % at b-time  $\sim 8 \mu\text{s}$ . At b-time =  $15 \mu\text{s}$  (chosen setting) the actual measured mean value of the blocking time (dead time) is  $\sim 20 \mu\text{s}$ .

## 4.5 Influence of SiPM dark count rate

Figure 10 shows how the trigger efficiency and the multi-count ratio of the detector are influenced by the dark count rate of the SiPM. The trigger probability is enhanced by the

presence of dark counts and both the trigger efficiency and the multi-count ratio increase with increasing the dark count rate. However, up to a dark count rate of  $\sim 2$  MHz the variation of these two parameters is minor.

## Summary

In this work we continued investigating the feasibility of the new approach, proposed in [3, 4, 5], to realize one-dimensional multichannel neutron detectors with ZnS:<sup>6</sup>LiF scintillators. In this approach the detector is built as an array of single-channel detection units containing scintillator with embedded WLS fibers readout by SiPMs. We built a prototype detection unit and performed characterization studies demonstrating the performance parameters to be similar to those of the currently used PMT-based detection systems [12, 13].

It is worth pointing out, that the compact size and the low price of SiPMs make the discussed approach feasible even in case of certain 2D-detectors. The large number of individual readout channels in such detectors will help solving the problem of their limited rate capability (remember, that the count rate per readout channel is limited by the necessity to introduce a certain dead-time in the detection process to cope with the long afterglow of the scintillator). This could be an option, for example, for large-area detectors for inelastic neutron scattering instruments where currently no adequate replacement to helium-3 detectors is found [1].

## Acknowledgments

We express our gratitude to Andreas Hofer (Detector Group of the Laboratory for Particle Physics) for designing and building our prototype detection units.

## References

- [1] K. Zeitelhack, Neutron News 23(4) (2012) 10.
- [2] N.J. Rhodes, Neutron News 23(4) (2012) 26.
- [3] J.-B. Mosset et al.,  
Journal of Physics: Conference Series 528 (2014) 012041.
- [4] A. Stoykov et al., 2014 JINST 9 P06015.
- [5] J.-B. Mosset et al., Nucl. Instr. and Meth. A 764 (2014) 299.
- [6] <http://www.appscintech.com>
- [7] <http://www.eljentechnology.com>
- [8] <http://kuraraypsf.jp>
- [9] <http://www.hamamatsu.com>
- [10] Y. Musienko et al., Nucl. Instr. and Meth. A 581 (2007) 433.
- [11] Saint-Gobain Crystals, PreLude 420 datasheet,  
[http://www.crystals.saint-gobain.com/PreLude\\_420\\_Scintillator.aspx](http://www.crystals.saint-gobain.com/PreLude_420_Scintillator.aspx)
- [12] T. Nakamura et al., Nucl. Instr. and Meth. A 600 (2009) 164.
- [13] T. Nakamura et al., Nucl. Instr. and Meth. A 686 (2012) 64.

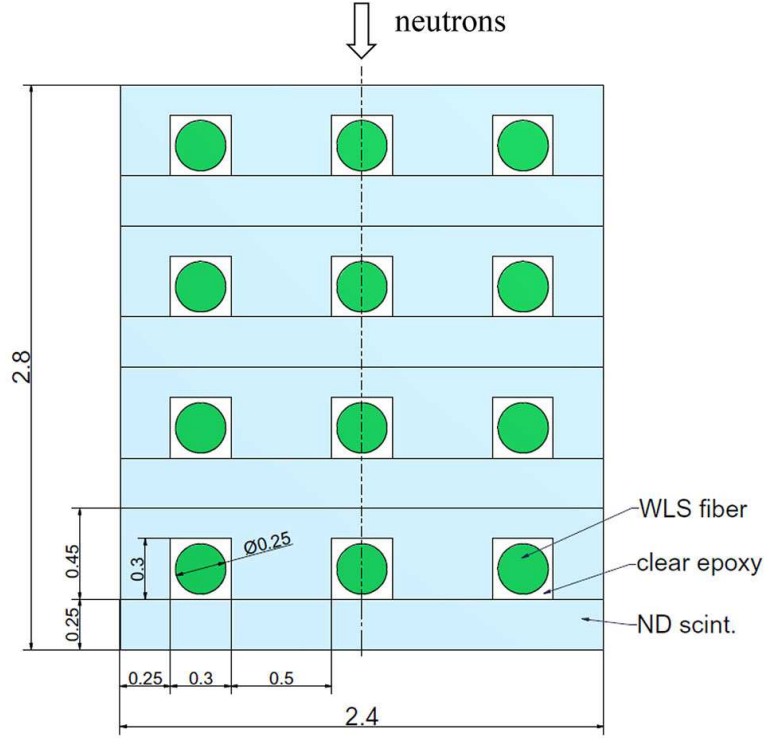


Figure 1: Cross-section of the sensitive volume of the detection unit. The scintillators are ND2:1 neutron detection screens from Applied Scintillation Technologies, the WLS fibers are of type Y11(400)M from Kuraray. The optical epoxy used to glue the fibers into the grooves and the scintillator sheets together is EJ-500 from Eljen.

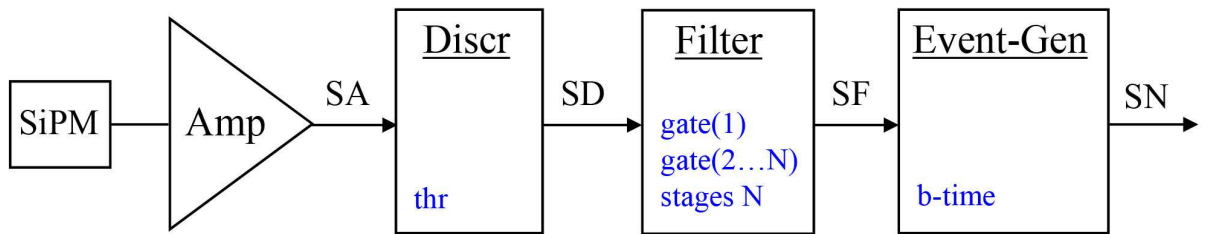


Figure 2: Processing scheme of the SiPM signals: high band-width amplifier, leading-edge discriminator, multistage filter, and event generator unit. The tunable parameters are: the discrimination threshold (thr), the number of filter stages (N), the retriggerable gate width of the first gate(1) and the following gate(2...N) filter stages, and the duration of the output pulse of the event generator (b-time blocking time) to account for the afterglow photons from the scintillation process.

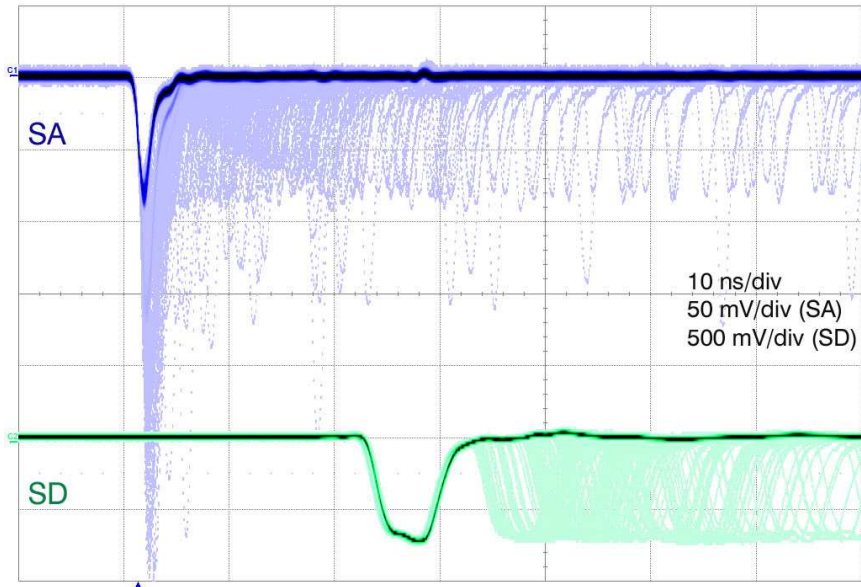


Figure 3: Conversion of the amplified and shaped SiPM analog signals (SA) into standard digital signals (SD) by a fast leading-edge discrimination stage. Note, that in contrast to the SA signals having admixture of the SiPM cell-to-cell cross-talk events (non-zero probability of signals with multiple amplitudes), the SD signals are free from any cross-talk contribution.

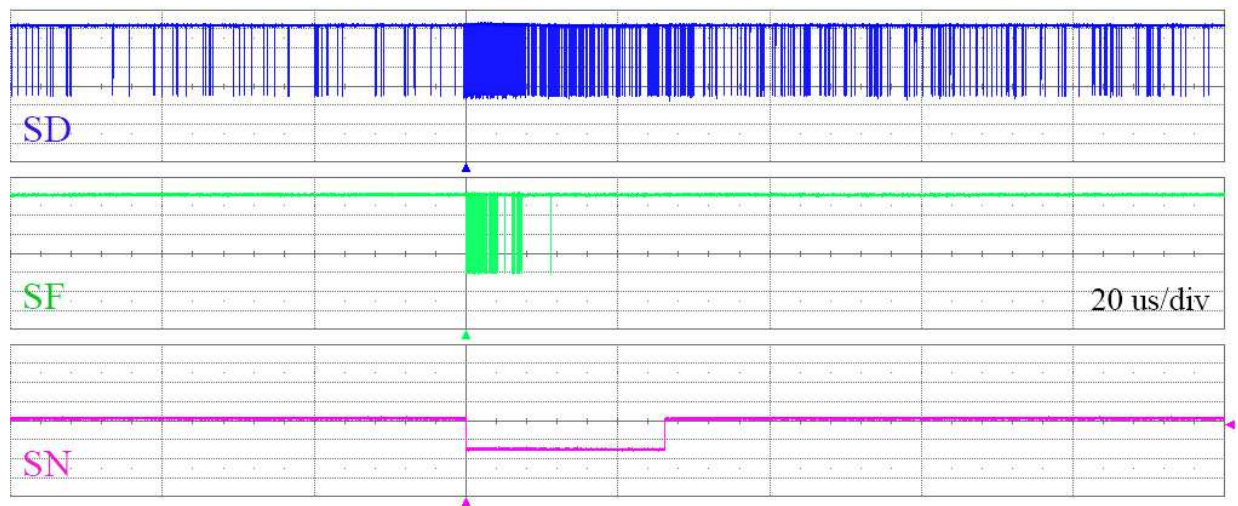


Figure 4: Detection of a neutron event: initial SD pulse sequence and the subsequence of SD-pulses passing the filter (SF-signal). The first pulse of the SF-sequence generates the leading edge of an event signal (SN). The set value for the width of the SN-signal is  $b\text{-time} = 15 \mu\text{s}$ , its actual width determined by the strength of the SF-signal is  $\sim 25 \mu\text{s}$ . The presented event is relatively strong: there are 238 SD-pulses within the first  $10 \mu\text{s}$  of the event, 113 of these pulses pass the filter. The filter settings are:  $N = 10$ ,  $\text{gate}(1) = 30 \text{ ns}$ ,  $\text{gate}(2 \dots N) = 500 \text{ ns}$ . The dark count rate of the SiPM is 1 MHz.

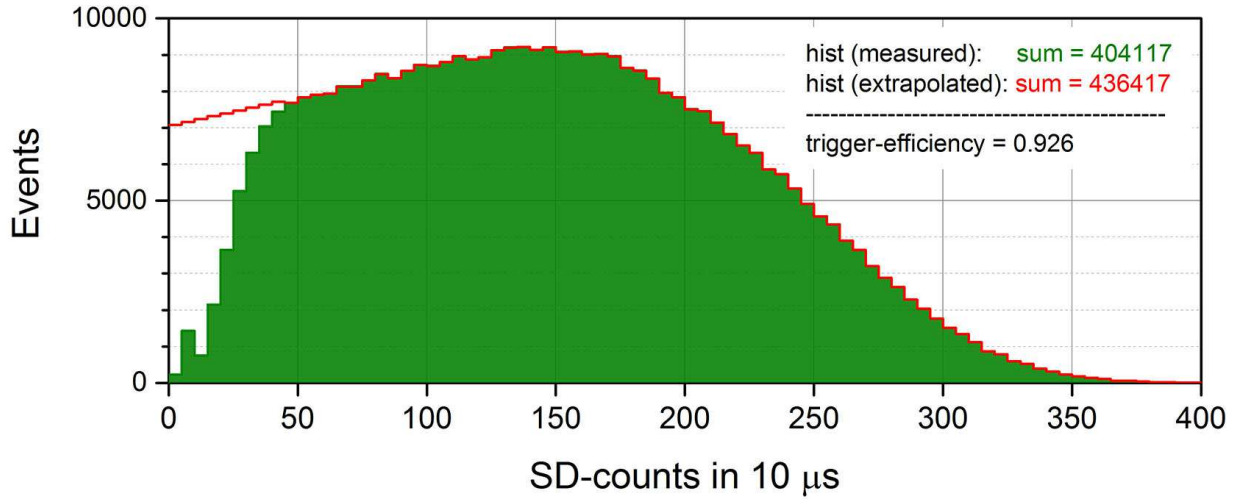


Figure 5: Calibration measurement to determine the neutron absorption rate in the detection unit. The detection threshold is set as low as possible:  $\text{gate}(1) = 80 \text{ ns}$ ,  $N = 4$ . Other parameters for the signal processing are:  $\text{gate}(2..N) = 500 \text{ ns}$ ,  $\text{b-time} = 100 \mu\text{s}$ . The SiPM dark count rate is  $100 \text{ kHz}$ . Shown is the measured histogram of the number of SD-counts within the first  $10 \mu\text{s}$  of the detected events and extrapolation of this histogram to zero number of SD-counts. The ratio of the number of events in the measured histogram to that in the extrapolated one gives the trigger efficiency of 0.92. Taking into account the measured event rate of  $8.3 \text{ Hz}$  the neutron absorption rate is estimated to be  $9.0 \text{ Hz}$ .

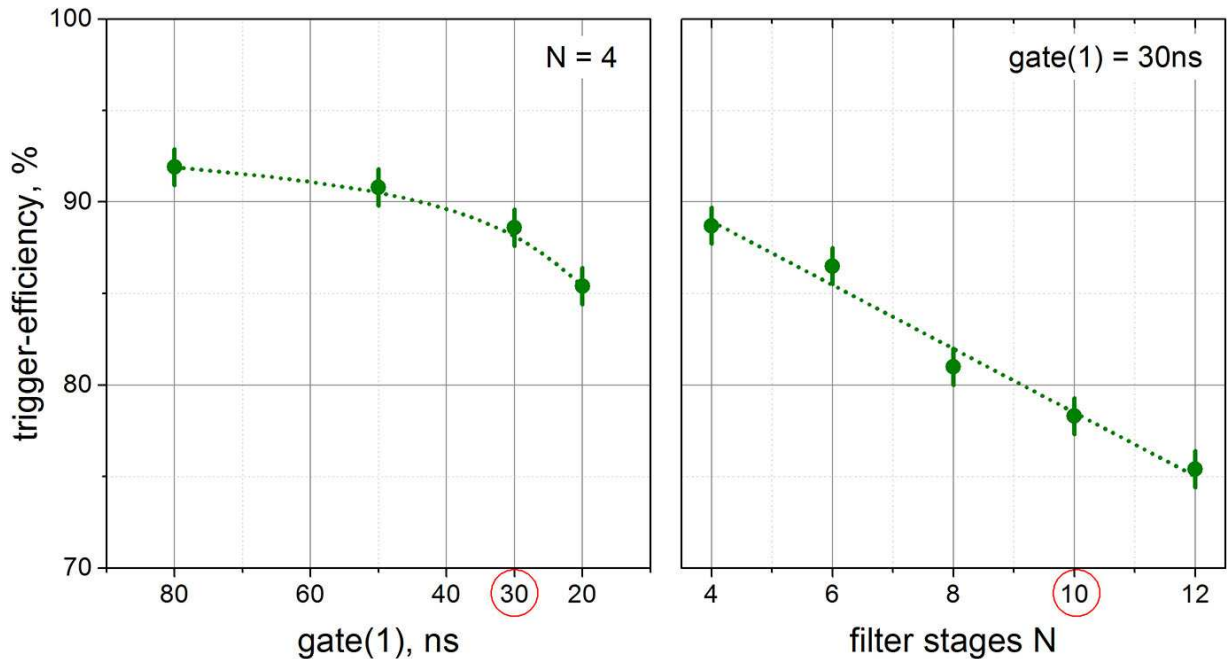


Figure 6: Trigger efficiency as a function of the gate width of the first filter stage  $\text{gate}(1)$  measured at  $N = 4$  (left) and of the number of filter stages  $N$  measured at  $\text{gate}(1) = 30 \text{ ns}$  (right). Other parameters for the signal processing are fixed at:  $\text{gate}(2..N) = 500 \text{ ns}$ ,  $\text{b-time} = 100 \mu\text{s}$ . The dark count rate of the SiPM is  $100 \text{ kHz}$ . The chosen filter settings are indicated by red circles. The dashed lines are shown to guide the eye.



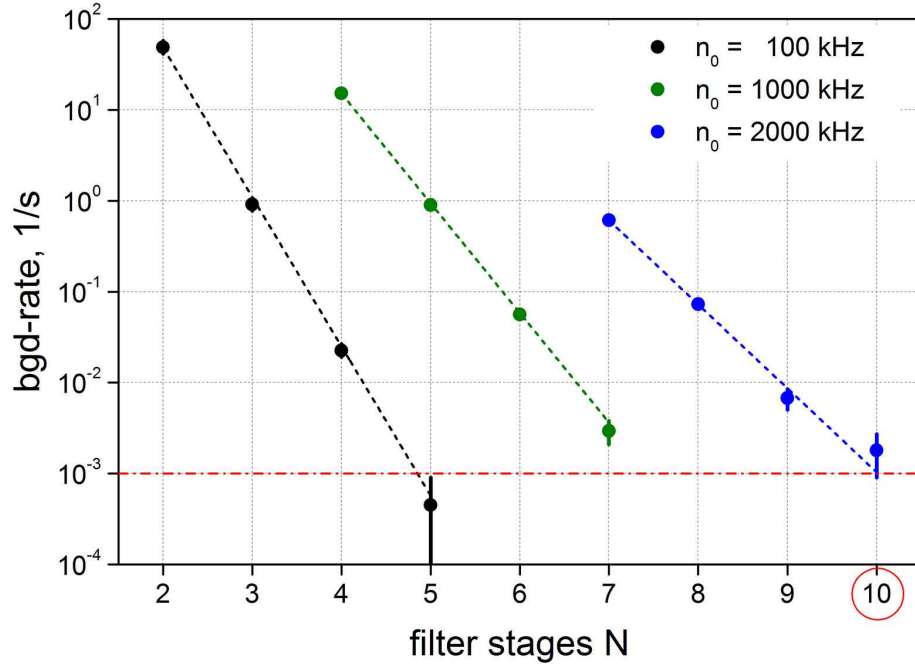


Figure 7: Background count rate of the detector as a function of the number of filter stages  $N$  at different values of the SiPM dark count rate. Other parameters for the signal processing are fixed at:  $\text{gate}(1) = 30$  ns,  $\text{gate}(2..N) = 500$  ns,  $\text{b-time} = 100$   $\mu\text{s}$ . The chosen filter setting is indicated by the red circle. The dashed lines are shown to guide the eye.

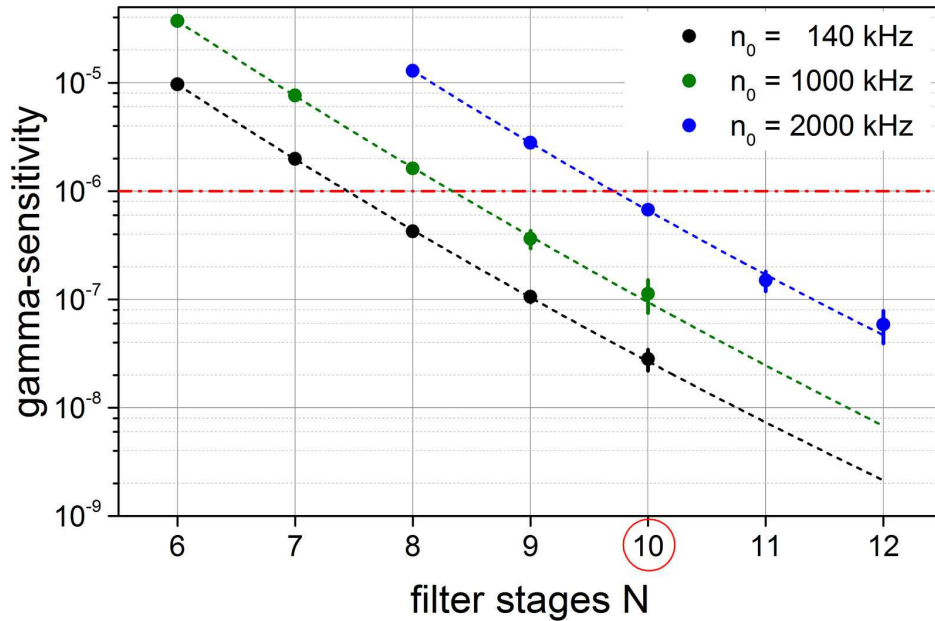


Figure 8: Gamma-sensitivity as a function of the number of filter stages  $N$  at different SiPM dark count rates. Other parameters for the signal processing are fixed at:  $\text{gate}(1) = 30$  ns,  $\text{gate}(2..N) = 500$  ns,  $\text{b-time} = 100$   $\mu\text{s}$ . The chosen filter setting is indicated by the red circle. The dashed lines are shown to guide the eye.

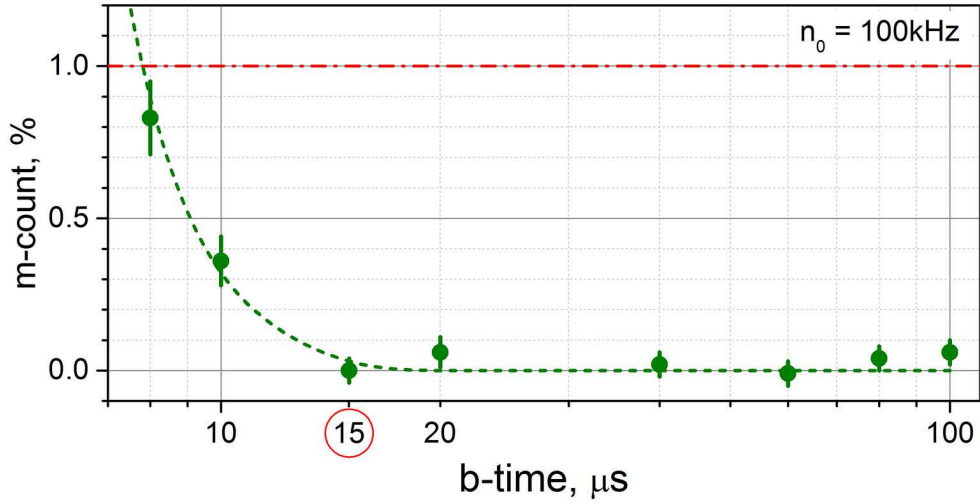


Figure 9: Multi-count ratio of the detector as a function of the set value of the blocking time of the event generator. Other parameters for the signal processing are fixed at:  $\text{gate}(1) = 30 \text{ ns}$ ,  $\text{gate}(2..N) = 500 \text{ ns}$ ,  $N = 10$ . The dark count rate of the SiPM is  $100 \text{ kHz}$ . The chosen b-time setting is indicated by the red circle. The dashed line is shown to guide the eye.

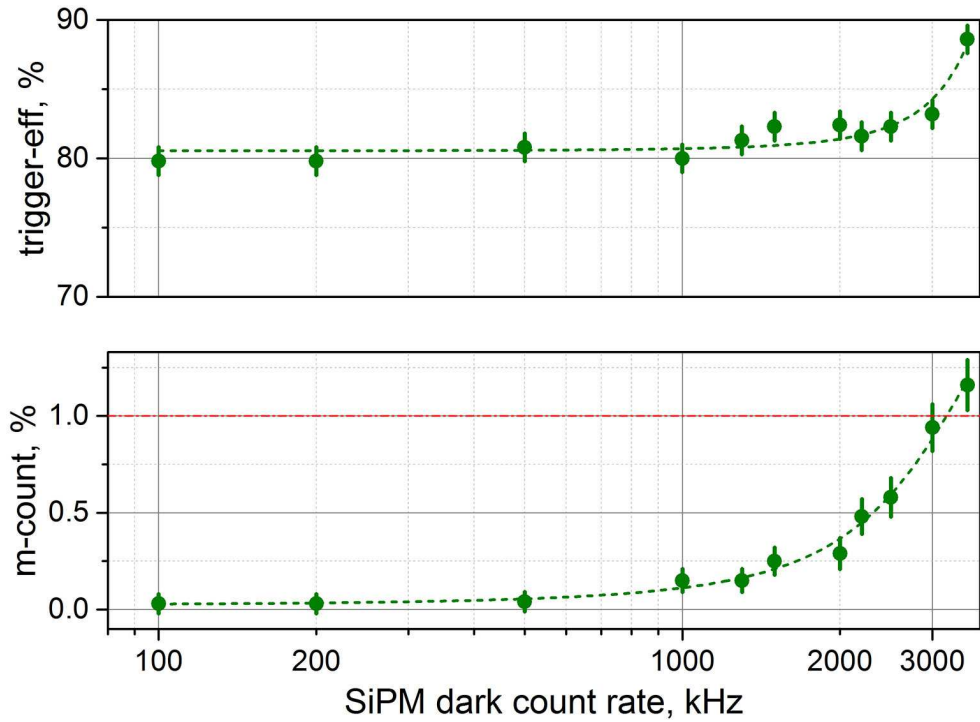


Figure 10: Trigger efficiency and multi-count ratio as a function of the dark count rate of the SiPM. The parameters for the signal processing are fixed at:  $\text{gate}(1) = 30 \text{ ns}$ ,  $\text{gate}(2..N) = 500 \text{ ns}$ ,  $N = 10$ ,  $\text{b-time} = 15 \mu\text{s}$ . The dashed lines are shown to guide the eye.